



Original article

Zinc's protective role against hydroxychloroquine-induced cardiac effects in adult male albino rats

Nihal A. Ibrahim^{a,b}, Manal A. Buabeid^{c,*}, El Shaimaa Arafa^{a,b}, Kadreya E. Elmorshedy^d^a Department of Clinical Sciences, College of Pharmacy and Health Sciences, Ajman University, UAE^b Centre of Medical and Bio-allied Health Sciences Research (CMBAHSR), Ajman University, Ajman, UAE^c Fatima College of Health Sciences, Department of Pharmacy, UAE^d Anatomy Department, Tanta College of Medicine, Egypt

ARTICLE INFO

Article history:

Received 30 May 2023

Revised 22 June 2023

Accepted 30 June 2023

Available online 4 July 2023

Keywords:

Hydroxychloroquine (HCQ)

Cardiomyopathy

Endocardium

Arrhythmia

Electron microscopy

Albino rat

Zinc

Myocardium

Telocytes

ABSTRACT

Background: Long exposure to Hydroxychloroquine (HCQ) has been complicated by some dangerous though infrequent cardiotoxicity.

Methods: A total of 40 normal adult male albino rats dispersed into 4 groups were used. Group 1 (Control group), Group II (HCQ treated group), Group III (zinc [Zn]-treated group), and Group IV (HCQ and Zn treated group). Once the experimentation ended, rats were sacrificed and cardiac soft tissue sections were processed twenty-four hours at the end of the experiment for histological study.

Results: Cardiac-stained sections revealed that HCQ induced widespread necrosis, dilatation, and vacuolar degeneration. However, the combination of HCQ with Zn ameliorated these damaging effects. Cardiac enzyme parameters were also studied in the 4 groups and revealed CK-MB and troponin were considerably elevated in groups II associated to the control group.

Conclusion: It was concluded that Zn revealed a protective role against HCQ cardiomyopathy in adult male albino rats. This might signify an appreciated means for Zn-based treatment in the upcoming subsequent clinical records to adjust doses and guarantee patient safeguard.

© 2023 The Authors. Published by Elsevier B.V. on behalf of King Saud University. This is an open access article under the CC BY-NC-ND license (<http://creativecommons.org/licenses/by-nc-nd/4.0/>).

1. Introduction

Chloroquine phosphate (CQP) and HCQ sulfate (HCS), are medications derived from 4-aminoquinolin compounds that are commonly prescribed for several diseases (Taherian et al., 2013). Although originally used as antimalarial drugs there has been growing interest in their potential use in treating other diseases such as cancer and viral infections including COVID-19 (Mubagwa, 2020). HCQ is often preferred over CQ due to its better tolerability at higher doses, and both drugs have similar beneficial and toxicological effects (Pasadhika & Fishman, 2010). However,

the use of these medications in the treatment of COVID-19 has raised concerns about their potential cardiotoxicity, which can cause ventricular arrhythmia, conduction disorders, and myocardial dysfunction (Kamp et al., 2020). Continued usage of HCQ has been associated with conduction disorders and myocardial dysfunction. Echocardiographic signs of HCQ cardiomyopathy are augmented thickening of ventricular wall and/or dilation with systolic or diastolic malfunction. Histopathological criteria in myocarditis are generic and revealed perivascular mononuclear infiltrates and myocyte cellular damage, additionally HCQ injuriousness was complemented by tissue vacuolization (Muthukrishnan et al., 2011; Hsieh et al., 2019).

Long-term use of CQ/HCQ may also induce myopathy, which may be due to the drugs' interference with lysosomal function and cell membrane stability. Histopathological analysis is crucial in diagnosing antimalarial cardiotoxicity resulting in congestive heart failure, myocardial dysfunction in addition to other complications (Costedoat-Chalumeau et al., 2007; Joyce et al., 2013; Naddaf et al., 2021). According to Klein et al., 2021 telocytes (TCs), a cell population that was first described only 16 years ago, made a significant contribution to the field of cardiovascular regeneration research in 2021. All layers of the heart wall contain

* Corresponding author.

E-mail addresses: n.ibrahim@ajman.ac.ae (N.A. Ibrahim), manal.buabeid@fchs.ac.ae (M.A. Buabeid), e.arafa@ajman.ac.ae (E. Shaimaa Arafa), kadreyaelmorshedy@med.tanta.edu.eg (K.E. Elmorshedy).

Peer review under responsibility of King Saud University. Production and hosting by Elsevier.



Production and hosting by Elsevier

<https://doi.org/10.1016/j.sjbs.2023.103733>

1319-562X/© 2023 The Authors. Published by Elsevier B.V. on behalf of King Saud University.

This is an open access article under the CC BY-NC-ND license (<http://creativecommons.org/licenses/by-nc-nd/4.0/>).

TCs, which are tiny cells with cytoplasmic protrusions known as telopodes that are incredibly long. TCs also secrete extracellular vesicles, such as exosomes (Diagram 1). Transmission electron microscopy (TEM) is a valuable technique for identifying ultra-structural changes in the heart, including mitochondrial abnormalities, autophagy, and mitophagy. TCs, a type of interstitial cell found in the heart and other organs, have been shown to possess c-kit positive cells with TC features in sub-epicardium, sub-epicardial arteries, sub-epicardial fat, the sub-endocardium, and between cardiac muscle bundles, as detected by immunohistochemistry and electron microscopy (Rusu et al., 2012; Iancu et al., 2018; Babaei et al., 2020; Collins et al., 2021). Zn has been suggested as a potential treatment for COVID-19, as oral Zn supplementation has been shown to reduce mortality, ICU admissions, and symptom duration. However, there is currently insufficient data to fully understand the effects of Zn on COVID-19 (Abdallah et al., 2023).

2. Materials and methods

2.1. Drugs

Sanofi Aventis Corporation provided HCQ phosphate tablets (Plaquenil 200-mg film-coated tablets), while Zn acetate tablets were obtained from Sigma company.

2.2. Animals and experimental design

This study was conducted with the approval of both AUREC and the Ethical Committee of Animal Researches of Ajman University (P-H-F-Jun-16). Forty adult male albino rats weighing between 180 gm. to 220 gm. were randomly divided into four groups, with 10 rats in each group. Both drugs were dissolved in distilled water and administered orally to the rats, with each rat receiving 1/10th of the LD50 dose of HCQ and 10 mg Zinc/kg body weight of zinc acetate per day for six weeks (MSDS, 2011). The dosages were adjusted weekly based on the rats' body weight. The rats were kept in hygienic, well-aerated cages with access to food and water and under the observation of an expert.

Group I (Control group):

Ten rats were given 1 ml of distilled water orally.

Group II (HCQ treated group):

Ten rats were given 124 mg/kg/b. of HCQ in a watery solution (equivalent to 1/10th of the oral LD50 in rats). The dosages were designed based on the rats' daily weights (Bastway et al., 2008).

Group III (Zn-treated group):

Ten rats were given 10 mg Zinc/kg body weight of zinc acetate by oral tube every day for the designated period.

Group IV (HCQ and Zn-treated group):

Ten rats were given both HCQ and Zinc according to the previously recommended doses. Twenty-four hours after the experimental periods, cardiac tissue and blood samples were collected by decapitating the rats.

2.3. Cardiac enzymes assessment

Serum samples were obtained from blood collected via orbital puncture, and cardiac biomarkers were assessed by measuring Creatine Kinase (CK-MB) and Troponin (cTnI) by ELISA kits at Al-Safwa laboratory center Ezeiruaku.F.C, 2019.

2.4. Histopathological studies

Heart biopsies were taken from all groups for histopathological assessment. Tissue specimens were fixed in 10% formaldehyde,

dehydrated in alcohol, and embedded in paraffin. Hematoxylin & Eosin staining was used to examine pathological alterations under a light microscope (Bancroft & Gamble, 2008 Wick, 2019; Elgharabawy et al., 2021). According to (Nour et al., 2017) immuno-histochemical study was conducted by CD-117 as a marker for TCs and angiogenesis by the way of Ye et al. (2007). Paraffin-embedded tissue slices were deparaffinized, and antigen retrieval was accomplished by warming the tissue slices at 96 °C in 0.01 mol/liter citrate buffer (pH 6.0) or EDTA solution (pH 8.0) for 20 min and freezing them to room temperature (Suvarna et al., 2018). Additionally, the heart was opened from the left ventricle and tiny cardio-myocytes samples were prepared for electron microscopic examination by the use of dissecting microscope. The tissues were fixed in 3% glutaraldehyde, followed by embedding in Araldite resin (Pogodina et al., 2006; Golomb et al., 2012). Ultrathin sections were examined using a JEOL-Jem.1400 (TEM) at the central research park of Al-Qassimi Center in Cairo University.

2.5. Statistical analysis methods

The statistical analysis of the complete records was conducted using the latest SPSS statistical software package, and the data were presented as Mean ± Standard deviation of Means (S.E.M). Group comparisons were made using a one-way ANOVA test, and a p-value of ≤ 0.05 was deemed statistically significant, while a p-value of > 0.05 was considered insignificant, according to (Ibrahim et al., 2021).

3. Results

3.1. Light microscopy

3.1.1. Hematoxylin and eosin stained sections

In the light microscopy sections, the Hematoxylin and eosin-stained (HX& E) sections of rat myocardium were examined. The control group showed bifurcating and anastomosing longitudinal muscle fibers with central oval nuclei. Some cells with elongated nuclei were also present (Fig. 1.A). However, the myocardium from group II (HCQ-treated group) exhibited myocytes with intensely eosinophilic cytoplasm and pyknotic nuclei. Areas of hemorrhage, focal zones of damage, and cytolysis of myocytes were observed. Additionally, cardiac myocytes displayed variations of wavy myofibrillar striated branched look, discontinuity by neighboring myofibrils and oval nuclei. There were also widespread cellular leukocyte infiltration and edema. Fibroblast-like cells with elongated nuclei were present (Fig. 1.B&C). Moreover, the cardiac myocytes of the same group showed vacuolations and pyknotic nuclei with widened areas among longitudinal cardiac muscle fibers and zones of degeneration. Fibroblast-like cells with elongated nuclei were also evident (Fig. 1.D). On the other hand, the sector of rat myocardium from group III (Zn treated group) and IV (HCQ and Zn treated group) showed cardiac myofibrils with normal striations and oval nuclei. Some cells with elongated nuclei were seen (Fig. 1.E&F).

3.1.2. CD 117 immuno-stained rat cardio-myocytes

Immunostaining for CD117 was performed on rat cardio-myocytes, and the results were as follows: The control group (I) displayed spindle-shaped TCs with CD117 expression, small nucleated bodies, and elongated moniliform telopodes in the interstitium between cardiac muscle fibers (Fig. 2. Panel A). In the HCQ-treated group (II), there was a dense meshwork of CD117 (+) TCs with prominent elongated moniliform telopodes adjacent to cardiac muscle fibers and sarcolemmal vacuolations (Fig. 2. Panel B&C). CD117 (+) network was observed within the myocardium

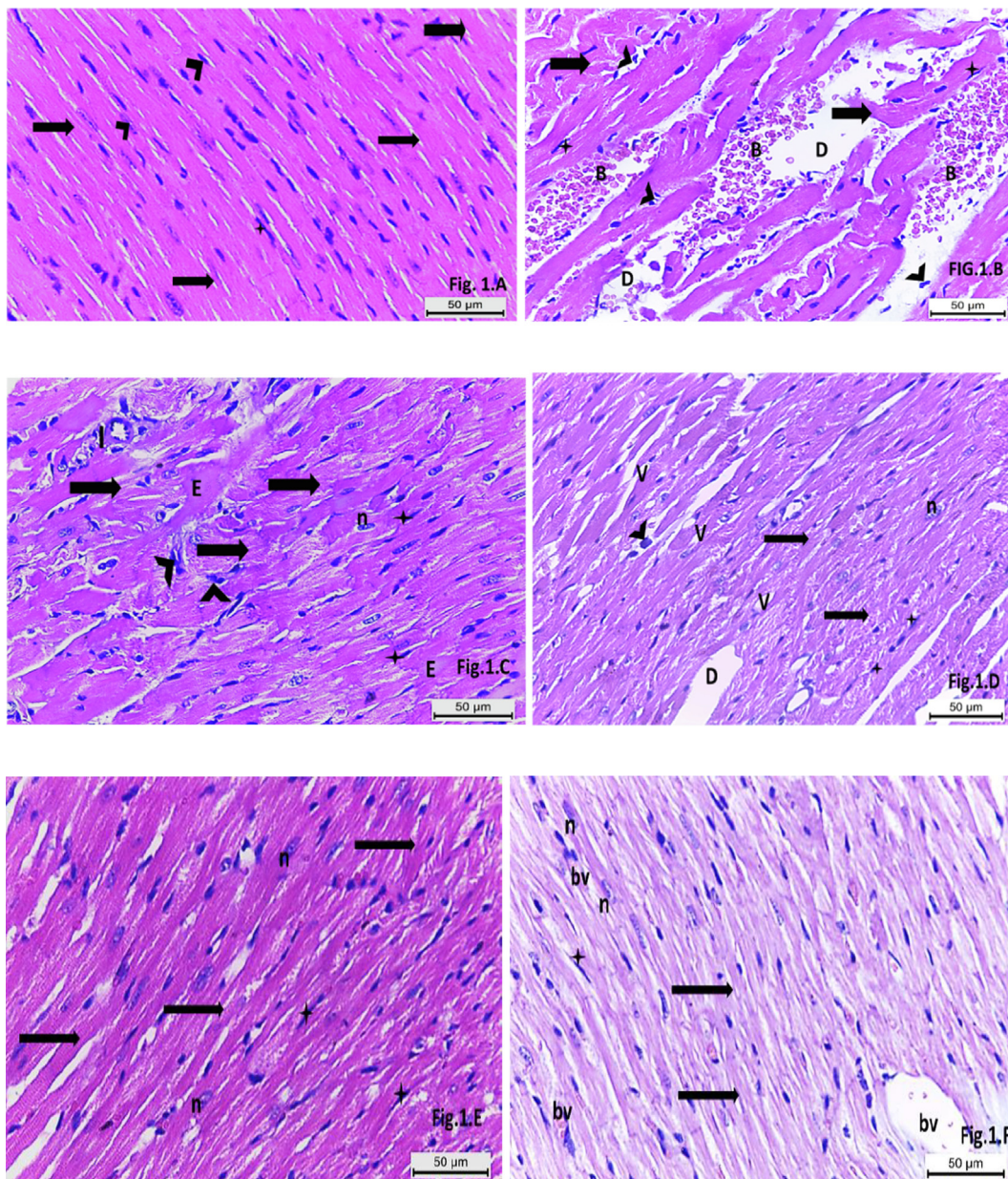


Fig. 1. Displays photomicrographs of sections of rat myocardium from different treatment groups. **Panel A** shows the control group, where the myocardium exhibits bifurcating and anastomosing longitudinal muscle fibers (arrows) with central oval nuclei (arrow heads). Cells with elongated nuclei (star) are also visible. **Panel B** shows myocardium from the HCQ-treated group (group II), where some myocytes have intensely eosinophilic cytoplasm (arrows) and pyknotic nuclei (arrow heads). The section also displays zones of hemorrhage and extravasated blood (B), as well as focal zones of damage and cytolysis of myocytes (D). Cells with elongated nuclei (star) are present. **Panel C** shows cardiac myocytes from group II with wavy myofibrils, striations (arrows), a branched look, discontinuity with neighboring myofibrils, and oval nuclei (n). Cellular leukocyte infiltration (I) and edema (E) are widespread, and fibroblast-like cells with elongated nuclei (star) are visible. **Panel D** shows cardiac myocytes from group II, where myofibrillar structures (arrows) exhibit vacuolations (V) and pyknotic nuclei (arrowheads). Widened areas between longitudinal cardiac muscle fibers with degeneration zones (D) are apparent. Fibroblast-like cells with elongated nuclei (star) are also visible. The photomicrographs were stained with hematoxylin and eosin and captured at a magnification of (HX. & EX400). **Panel E:** Section of rat myocardium from group III (Zn treated group) presenting cardiac myofibrils with normal striations (arrows) and oval nuclei (n). Cells with elongated nuclei (star) could be seen. **Panel F:** Section of rat myocardium from group IV (HCQ and Zn treated group) displaying cardiac myofibrils with typical striations (arrows) and oval nuclei (n). fibroblast like cells with elongated nuclei (star) and blood vessels (bv) could be seen.

of the Zn-treated group (III), with classic TC morphology and elongated telopodes present in spindle-shaped cardiac muscle fibers intervening in the interstitium (Fig. 2 Panel D). In the HCQ and Zn treated group (IV), CD117 (+) mast cells (MCs) were located in the vicinity of regenerated myocardial bundles with telocytes having telopodes giving a starry sky look. CD117 (+) immune reactivity was also present in blood vascular endothelium and in-between recovered cardiac muscle fibers (Fig. 2. Panel E&F).

3.1.3. Semi-thin stained sections of rat cardio-myocytes

Semi-thin sections of rat myocardium stained with toluidine blue revealed different features in the experimental groups. In the control group (I), normal myofibril striations with oval nuclei and Z-line connections were observed, along with visible blood vessels (Fig. 3. panel A&B). HCQ treatment (II) resulted in wavy myofibrils with fragmented zones, denuded and wavy myofibrils, as well as the presence of sarcolemmal vacuoles containing

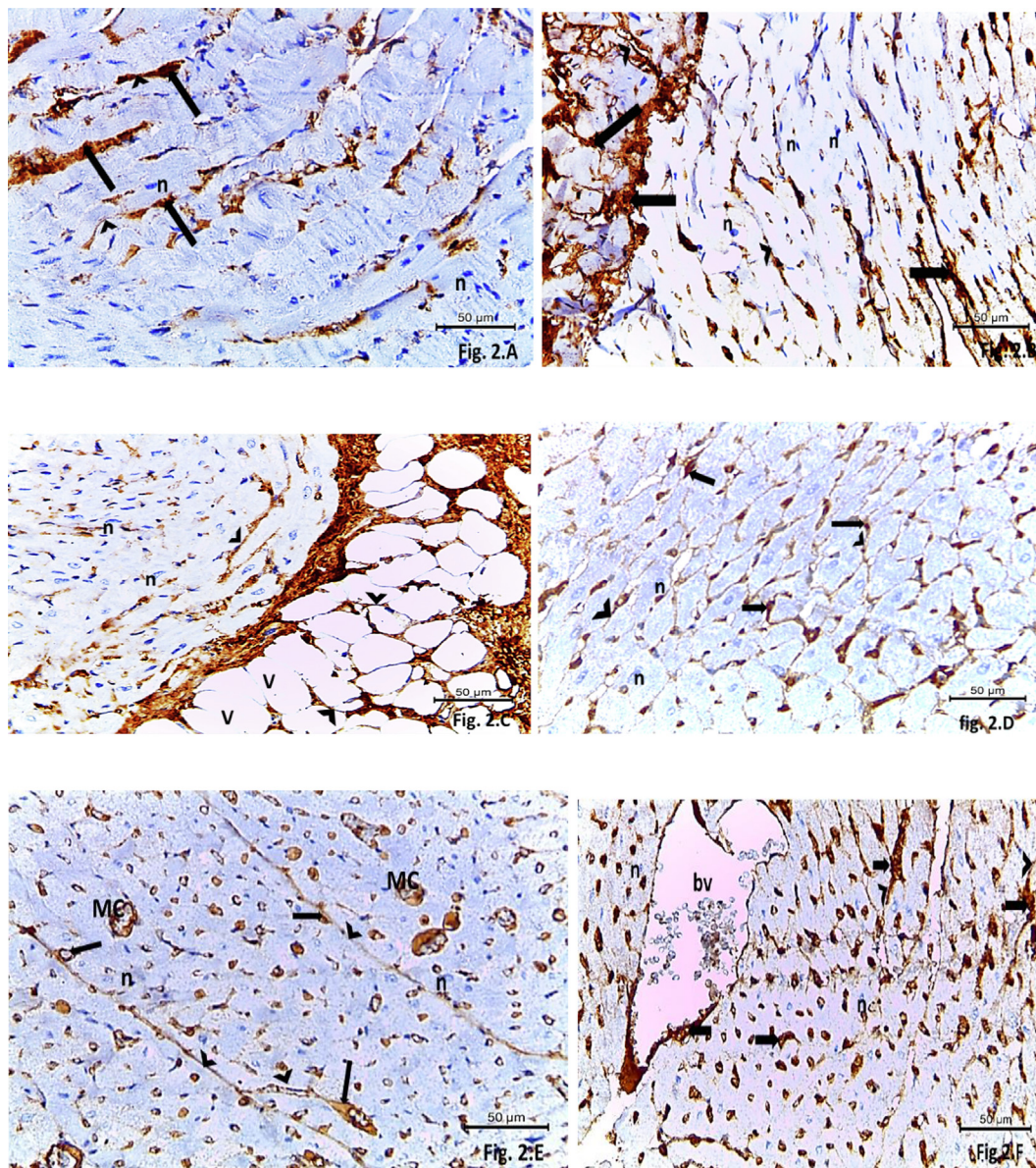


Fig. 2. Photomicrographs of CD 117 stained of rat cardio-myocytes: In **panel A** of the control group (I) classic CD117(+) spindle-shaped cells TCs (arrows), small nucleated bodies, and very elongated and thin moniliform processes (telopodes) (arrow heads) are observed in the intersitium between cardiac muscle fibers with oval nuclei(n). In **panel B** of the HCQ treated group (II), there is a compact meshwork of CD117 (+) TCs (arrows) with prominent elongated and moniliform telopodes (arrow heads) that closely interfaced with cardiac muscle fibers of oval nuclei(n). In **panel C** of the HCQ treated group (II), a dense meshwork of CD117 (+) TCs (arrows) with long and moniliform telopodes (arrow heads) are detected within sarcolemmal vacuolations (V). In **panel D** of the Zn treated group (III), a CD117 (+) network is found within the myocardium. Classic TC morphology (arrows) with spindle-shaped cells, small nucleated bodies, and very elongated and thin moniliform processes (telopodes) (arrow heads) are observed in the interstitium between spindle shaped cardiac muscle fibers with oval nuclei (n). (CD 117x400). **Panel E:** CD 117 (+) mast cell (MC), placed in the neighborhood of regenerated myocardial bundles (n), telocytes (arrows) with telopodes (arrow heads) giving a starry sky look. **Panel F:** CD117 (+) immune-reactivity (arrows) is identified also in blood vascular endothelium (bv) and in-between recovered cardiac muscle fibers(n).

lipofuscin-like granules. Crucial zones of myofibrillar breakdown and congested, dilated blood vessels were also noted, along with elongated cells branched extensions (Fig. 3. panel C&D). Cardiac myofibrils with oval nuclei surrounded by clear spaces, zones of myofibrillar degeneration with congested blood vessels surrounded by cellular infiltrate and branched TCs with intervening oval nuclei were also noticed (Fig. 3. panel E&F). In group III (Zn-treated), semi-thin sections displayed normal myofibril striations with oval nuclei connected by Z-lines, as well as a linear arrangement of mitochondria (Fig. 3. panel G). Group IV, treated with both HCQ and Zn, showed approximately normal myofibrillar structure with oval nuclei and visible Z-lines, but with the pres-

ence of a congested dilated blood vessel (Fig. 3. panel H). Overall, the semi-thin sections revealed various differences between the experimental groups in myofibril structure and blood vessel appearance.

3.2. Transmission electron microscopy (TEM)

The TEM images of the control rat cardio myocytes (group I) displayed typical arrangement of myofibrillar sarcoplasm with a central oval nucleus containing a prominent nucleolus. The myofibrils had even transverse striations bisected by Z lines, and regular rows of mitochondria were clearly visible. The myofilaments were

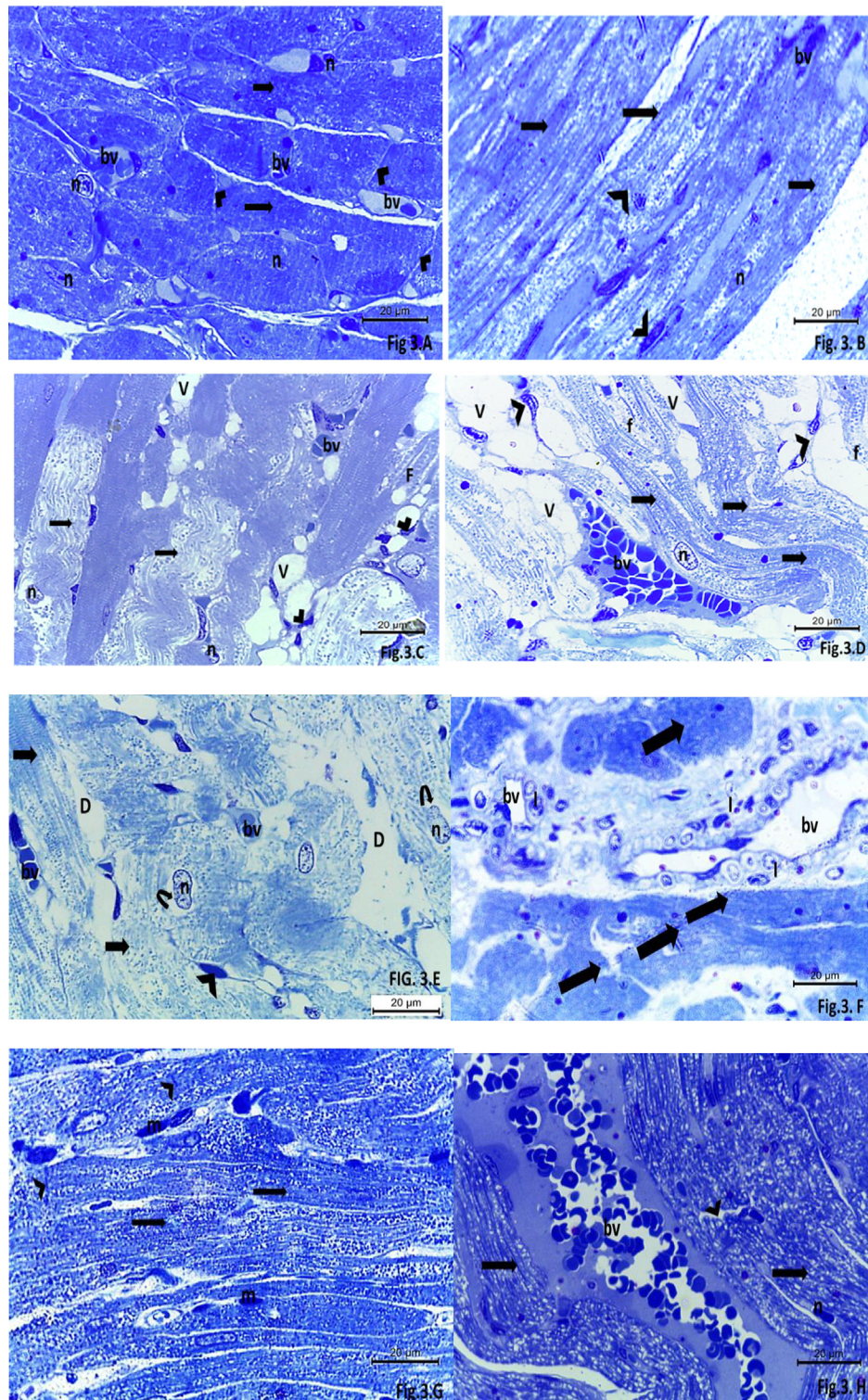


Fig. 3. panel A&B: Photomicrographs of a semi-thin section of control rat myocardium displaying standard striations of myofibrils (arrows) of oval nuclei (n) and their edges are connected with Z-lines (arrow heads). Blood vessels (bv) are evident. HCQ treated rat myocardium (group II) presenting: **panel C:** Curly cardiac myofibrils (arrows) with oval nuclei (n) and fragmented zones (f). Blood vessels (bv) are clearly seen. Sarcolemmal vacuoles (V) containing lipofuscin-like granules (arrow heads) are seen. **panel D:** Crucial zones of myofibrillar break down with focal loss of cross striations (F). Other myofibrils appear wavy and denuded (arrows). Notice congested dilated blood vessels (bv). Sarcolemmal vacuoles are clearly seen (V). elongated cells with branched extensions (arrow heads) are scattered between sarcolemmal vacuolizations. (Toluidine blue X 1000). **panel E:** Cardiac myofibrils (arrows) with oval nuclei (n) surrounded by clear spaces (curved arrows). Zones of myofibrillar degeneration (D) with congested blood vessels (bv) and branched TCs with intervening oval nuclei (arrow head). **panel F:** Irregularly arranged cardiac myofibrils (arrows) and dilated congested blood vessels (bv) surrounded by cellular infiltrate (I) are clearly seen. **panel G:** A photomicrograph of heart biopsy specimen from Zn treated group (III) treated rats showing normal striations of myofibrils (arrows) with Z-lines (arrow head) and oval nuclei (n). Notice linear arrangement of mitochondria (m). **panel H:** Photomicrograph of cardiac myocytes from HCQ and Zn treated group (IV) showing more or less normal myo-fibrillar structure (arrows) with oval nuclei (n). Z-lines (arrow head) is evident between myo-fibrillar edges. A congested dilated blood vessel (bv) could be seen. (Toluidine blue X 1000).

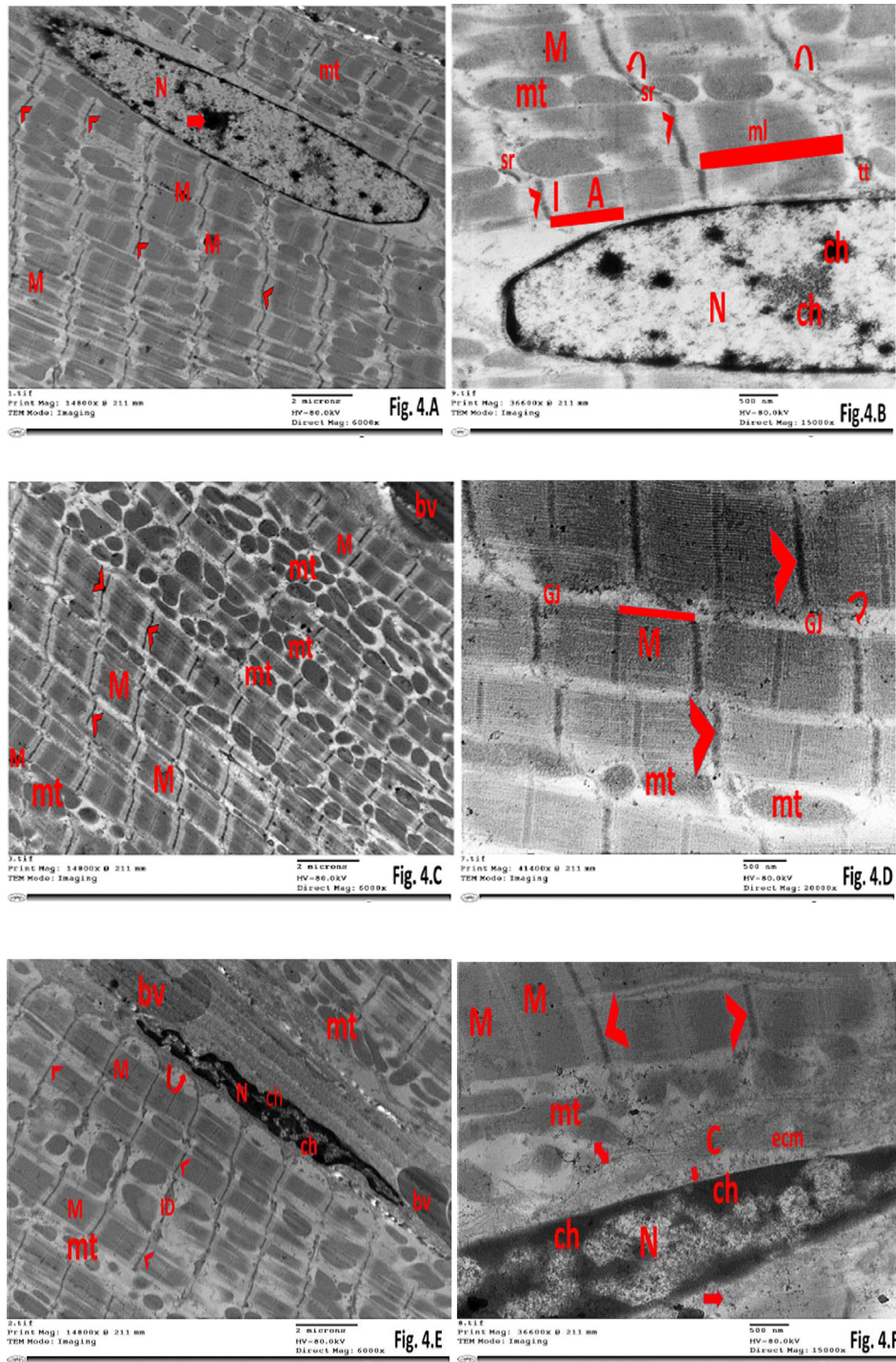


Fig. 4. Electron micrographs of control cardiac myocytes from rats in group i are presented. the following details can be observed:(A) The sarcoplasm of the myofibrils exhibits a regular arrangement of myofibrils (M) with transverse striations bisected by Z-lines (arrow heads) and even rows of mitochondria (mt) surrounding the centrally located nucleus (N) with a prominent nucleolus (arrow). (TEM X6000). (B) The myofilaments are regularly arranged in sarcomeres (■) with transverse striations (M) consisting of dark (A) and light (I) bands that intersect at Z-discs located near the steps that line up axially edge-to-edge with the intercalated disc (ID) (curved arrow). Mitochondria (mt) are present in columns parallel to the myofibrils that end at the verge of the ID. The sarcoplasmic reticulum (sr) is present between the mitochondria and ID membrane. In addition, regular myofilaments (M) connected by desmosomes (curved arrow), the cardio-myocyte nucleus (N) with extended chromatin (ch), and T-tubules (tt) can be seen. The middle line of the sarcomere (ml) is visible. (TEM X 15000). (C) The regular arrangement of myofilaments (M) bisected by Z-lines (arrowheads), blood vessel (bv), and even rows of mitochondria (mt) are evident. (TEM X 6000). (D) The myofilaments (M) are arranged in sarcomeres (■) with a gap junction (Gj) associated with coated pit (curved arrow) and transverse striations consisting of dark and light bands bisected by Z lines (arrowheads). Rows of mitochondria (mt) with their tube-like packed projecting cristae can also be seen. (TEM X 20000). panel E: An intact intercalated disc (ID) in-between myocytes (M) with a step-like pattern connected by Z lines (arrow heads). Regular rows of mitochondria (mt) and TC like cell with elongated nucleus (N) and dark peripheral chromatin (arrows), cell membrane (curved arrow) and blood vessels (bv) are seen. (TEM X6000). panel F: A TC with elongated nucleus (N) and peripherally condensed chromatin (ch) surrounded by a narrow cytoplasmic rim (arrows). Collagen deposition (C) in the extra-cellular matrix (ecm) with telopodes (double heads arrows) are clear. A nearby row of elongated mitochondria (mt), cardiac myofibrils (M) connected by Z-lines (arrow heads) are clearly seen. (TEM X15000).

arranged in sarcomeres with a step-like pattern, intersected by Z-discs, and lined up axially edge to edge with the intercalated disc (ID). The mitochondria ran parallel to the myofibrils and ended at the verge of the ID, while the sarcoplasmic reticulum was located between the mitochondria and ID membrane. The images also revealed regular transverse myofilaments arranged in sarcomeres with gap junctions associated with coated pit. The even transverse striations of myofibrils were made of dark and light bands bisected by Z-lines, and regular rows of mitochondria with their

tube-shaped packed projecting cristae were evident (Fig. 4. panel A, B&C). The ID between myocytes had a step-like design connected by Z lines. Furthermore, the images showed regular rows of mitochondria, a transitional cell-like structure with an elongated nucleus containing dark peripheral chromatin, cell membrane, and blood vessels. They also revealed cardio myocytes with myofibrillar sarcoplasm with a classic arrangement, a central oval nucleus with a prominent nucleolus, and even transverse striations of myofibrils bisected by Z lines. Regular rows of mitochondria and

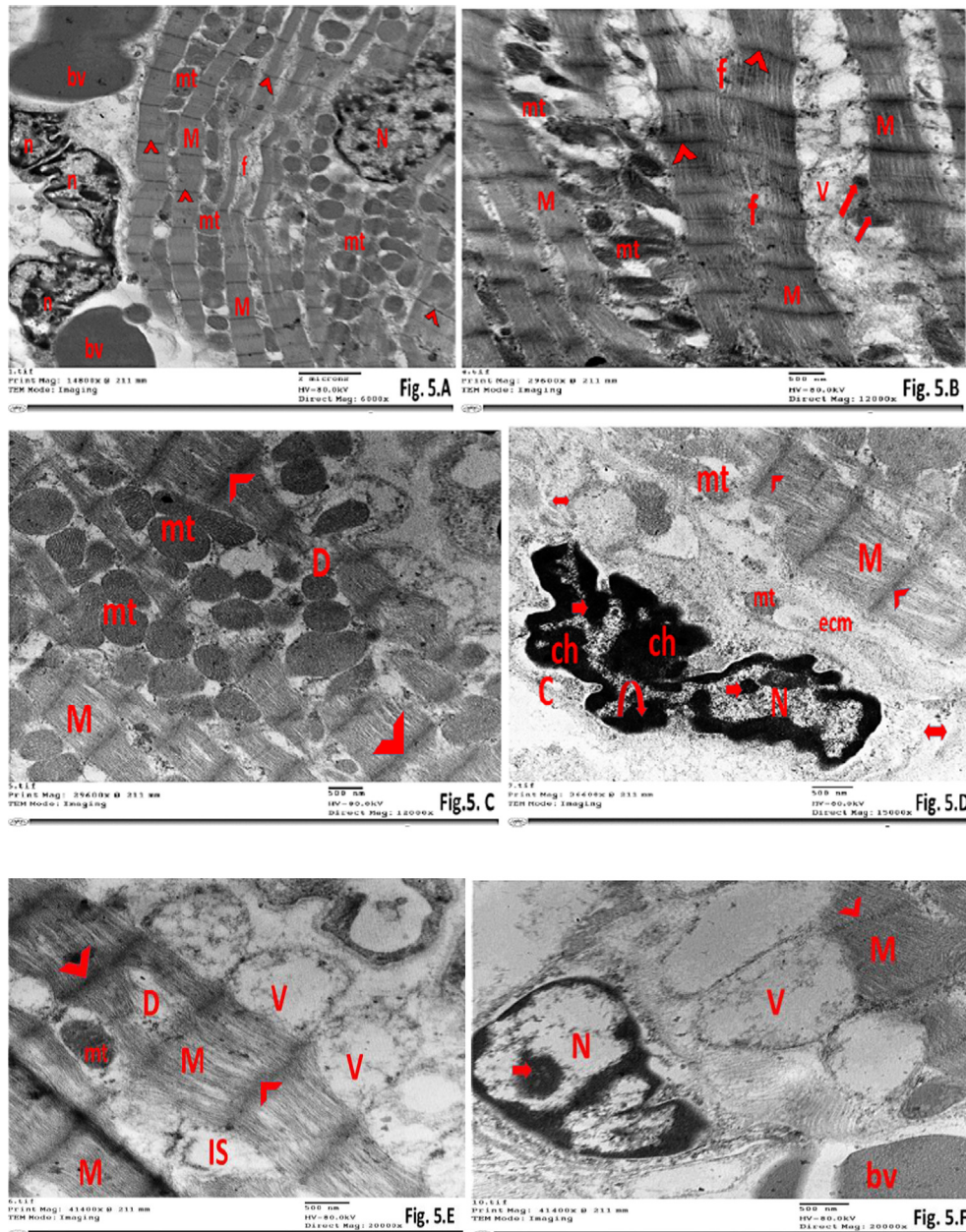


Fig. 5. TEM images of cardiac myocytes from the group treated with HCQ (group II) depict: **(A)** Irregular arrangement of myofibrils (M) in cardiac cells bisected by Z-lines (arrow heads) with localized areas of fragmentation (f) and irregular-shaped nucleus (N) with extended chromatin, surrounded by swollen mitochondria (mt). Leucocytic cellular infiltration with irregular nuclei (n) near neighboring blood vessels (bv) are visible. **(TEM X6000).** **(B)** Fragmentation (f) and damage to the regular organization of myofibrils (M) showing a bamboo-like shape with dark Z-lines between adjacent myocytes (arrow heads). The presence of vacuoles (V) and clusters of curvycircular bodies (arrows) in between the cells is noticeable. Dilated and compact mitochondria (mt) with uneven shapes and arrangement can be seen. **(TEM X12000).** **(C)** Disorganized cardiac myofibrils (M) with dark Z-lines between adjacent cells (arrow heads). Regions of degeneration (D) and unevenly arranged mitochondria (mt) of variable sizes with prominent cristae inside are visible. **(TEM X12000).** **(D)** A Tc nucleus (N) in a division state with two nucleoli (arrows) and condensed chromatin at the periphery (ch). Telopodes (double arrow) arising from the Tc extremities are visible. Collagen deposition (C) in the extracellular matrix (ecm), separated myofilaments (M) with dark Z-lines (arrow heads) between sarcomere edges, and few mitochondria (mt) can be seen. **(TEM X15000).** **panel E:** Accumulation of interstitial (IS) fluid and loss of regular arrangement of myofibrils (M) with Z-lines in-between (arrow heads) and degenerated areas (D). Swollen circular mitochondria (mt); some of which are vacuolated (V). **(TEM X20,000).** **panel F:** Fragmentation and loss of regular arrangement of myofibrils (M) with vacuoles (V) and Z-lines in-between (arrow heads). Irregular shrunken nucleus (N) with prominent nucleolus (arrow head) near a blood vessel (bv). **(TEM X20,000).**

myofilaments arranged in sarcomeres with dark and light bands intersected by Z-discs were clearly visible. The columns of mitochondria were parallel to the myofibrils and ended at the verge of the intercalated disc (ID) membrane, while the sarcoplasmic reticulum was crammed between mitochondria and ID membrane.

Furthermore, an integral ID between myocytes with a step-like design connected by Z lines, and regular rows of mitochondria were seen. In addition, there were gap junctions associated with coated pit and even transverse striations of myofibrils made of dark and light bands bisected by Z lines (Fig. 4. panel D). An intact

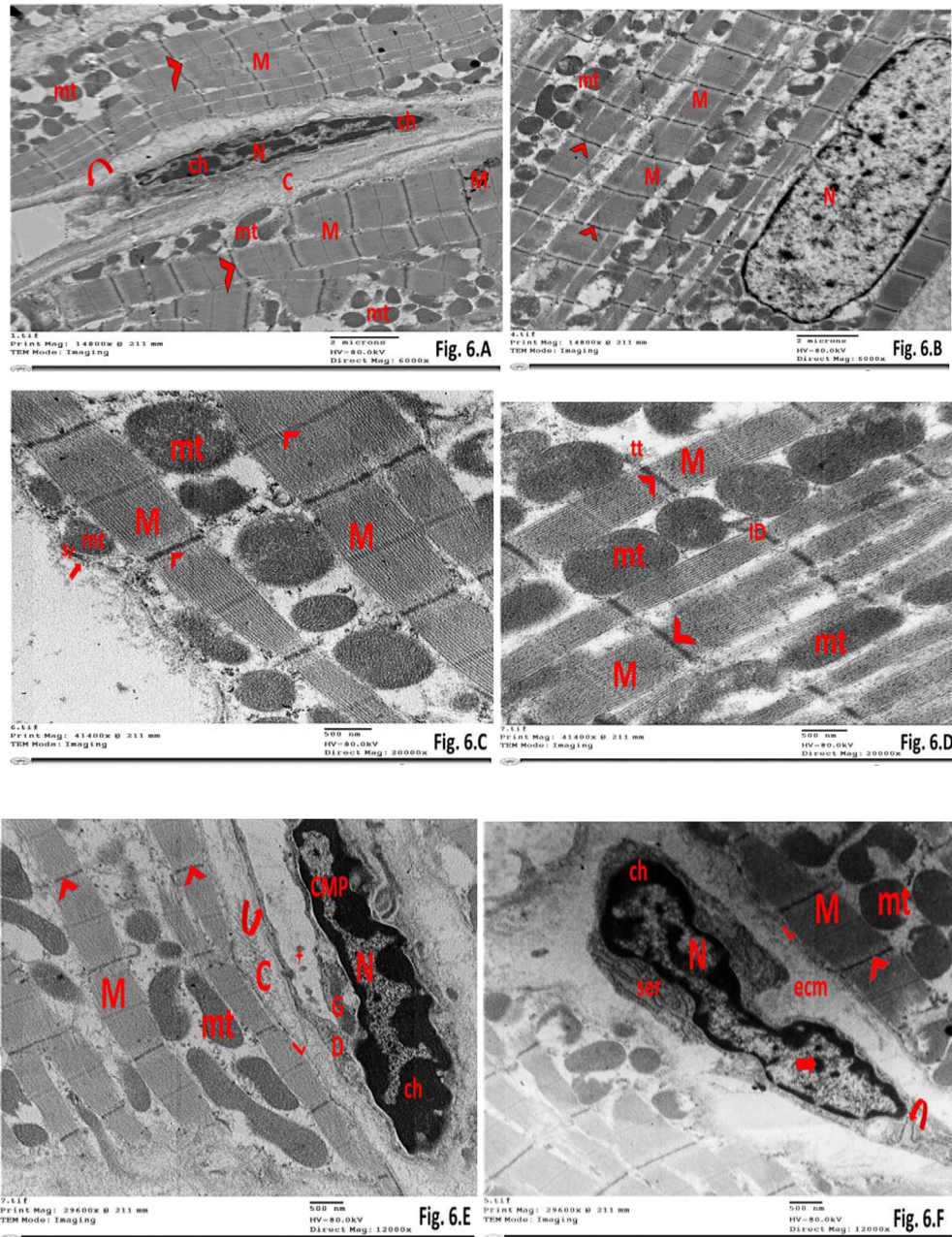


Fig. 6. The TEM micrographs from Zn-treated rat myocardium (group III) display the following: **(A)** Regularly arranged muscle fibers (M) with normal striations and Z-lines in between (arrow heads). The mitochondria (mt) are arranged in regularly spaced rows. The interstitium shows an elongated nucleus (N), which is most commonly a TC with peripherally condensed chromatin (ch) and a long process or telepole (curved arrow). Collagen deposition (C) is visible in the extracellular matrix between TC and cardiac myofibrils. **(TEM X 6000).** **(B)** Cardio-myocytes (M) with an oval nucleus (N) that exhibits extended chromatin. Z-lines (arrowheads) between cardio-myocyte edges and rows of oval mitochondria (mt) in between are visible. **(TEM X 6000).** **(C)** Cardiac myofibrils (M) with a regular arrangement of myofilaments linked by Z-lines (arrowheads), regular rows of mitochondria (mt) parallel to the myofibrils, and sarcoplasmic reticulum (sr) visible between mitochondria and the external lamina (arrow). **(TEM X 20000).** **(D)** Z-lines (arrowheads) between the edges of cardio-myocytes (M) with regular rows of rectangular mitochondria (mt) laid in between, ending at the intercalated disc region (ID) and t-tubules (tt). **(TEM X 20000).** **panel E:** Cardio-myocyte progenitor cell (CMP) with elongated nucleus (N) showing peripherally condensed beaded chromatin (ch) and small developing Golgi (G) and vesicles (star). Cardio-myocyte fibrils (M) are connected by Z-lines (arrow heads) with rows of elongated mitochondria (mt) in-between. Basal lamina (L) of cardio-myocytes encloses the CMP cell wall (curved arrow). Poorly differentiated desmosome (D) and reduced electron-dense collagen material (C) in a gap between contacting membranes of CMP and cardio-myocytes. **(TEM X 12,000).** **panel F:** Elongated nucleus (N) of TC present in a loose extracellular matrix (ecm) with prominent nucleolus (arrow) and peripherally condensed chromatin (ch) with telepole (curved arrow) and smooth endoplasmic reticulum (ser). TC is separated from cardio-myocytes (M) by cardiac external lamina (L) and loose extracellular matrix (ecm). Cardio-myocytes are connected by Z-lines (arrow heads) with regular rows of mitochondria (mt) in-between. **(TEM X 12,000).**

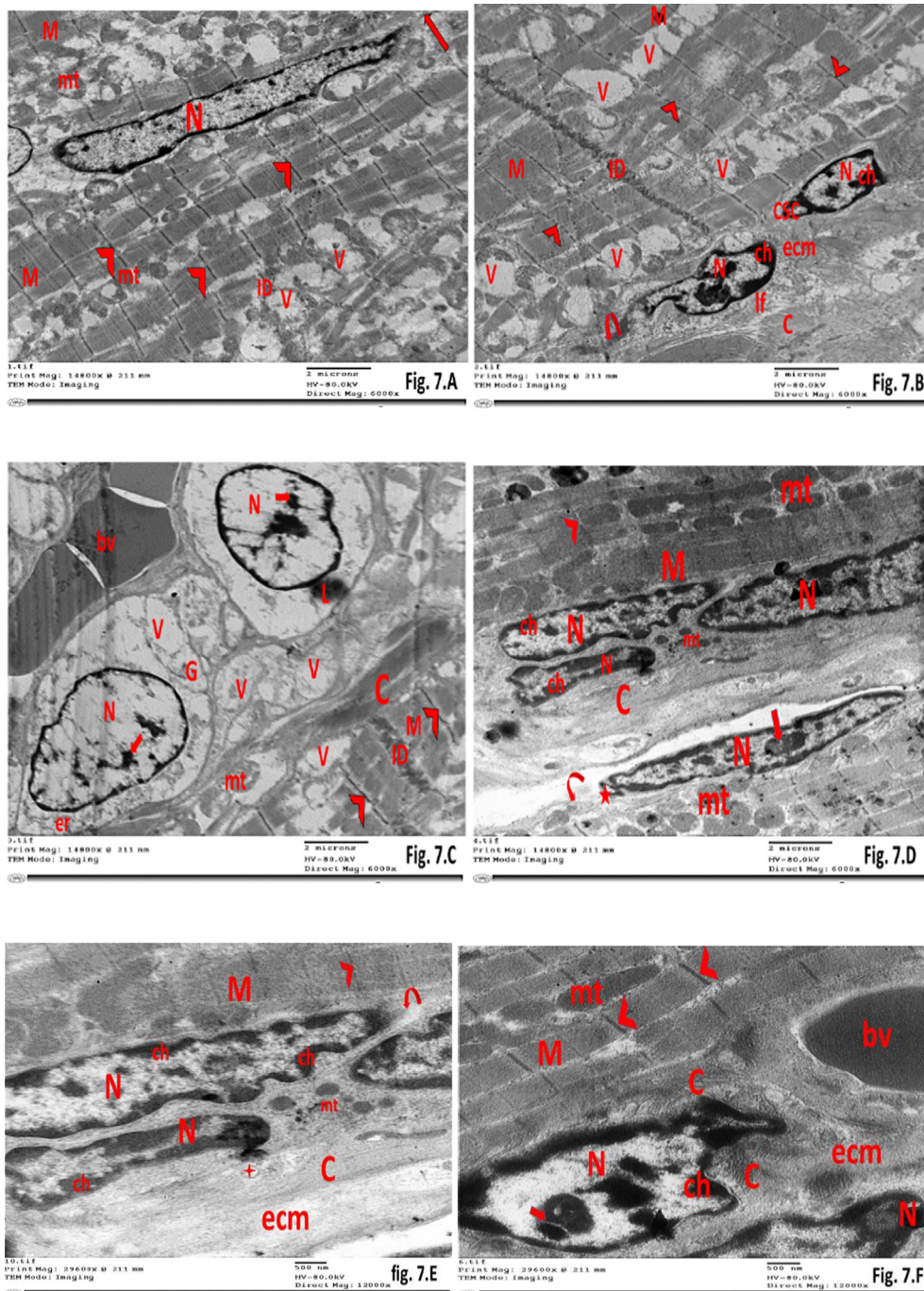


Fig. 7. The TEM micrographs in Fig. 7 show the effects of combined HCQ and Zn treatment on rat myocardium (group IV) as follows: **(A)** The image displays intact cardiac myofibrils (M) with swollen mitochondria (mt), and vacuolated sarcoplasm (V) with intact rows of intercalated discs (ID). Notice the classic Z-band (arrow heads) between cardio-myocyte edges. An elongated nucleus (N) of a TC with telopode (arrow) is visible. **(TEM X 6000).** **(B)** The micrograph exhibits a regular arrangement of myofibrils (M), some of which are vacuolated (V) connected by Z-lines (arrow heads). Integral intercalated discs of step-like design (ID) are visible. Two elongated nuclei (N) of cardiac stem cells (CSC) located in a loose extracellular matrix (ECM) with peripherally condensed chromatin (ch). The CSC of typical leptofibrils (lf) is closely supported by Tc processes (curved arrow). Extracellular collagen (C) is laid next to them. **(TEM X 6000).** **(C)** The image shows a regular arrangement of myofibrils (M) connected by Z-lines (arrow heads) and integral intercalated discs (ID) with a step-like design. Two cardiac stem cells located near a blood vessel (bv) with two large and dented nuclei, fewer dispersed chromatin, and prominent nucleoli (arrow). Endoplasmic reticulum (ER), collections of minor and clear vacuoles (V) creating a multi-locular look, scarce condensed granules (G), and lysosomes (L) are seen. Extracellular collagen (C) is laid between cell outlines and cardiac myofibrils. **(TEM X 6000).** **(D)** This micrograph displays typical TCs with elongated nuclei (N) which contains heterochromatin in their periphery (ch) and prominent nucleoli (arrow). Their cytoplasm contains small mitochondria (mt) and vesicles (star) in the podoms (curved arrow). The TCs are located near cardio myocytes (M) that are connected by Z-lines (arrow head) with regular rows of mitochondria (mt) arranged in between. **(TEM X 6000).** **(E)** A magnified photomicrograph of the previous one showing typical TCs with elongated nuclei (N) with peripherally condensed chromatin (ch) giving a beaded appearance and numerous shed extracellular vesicles (star) in the connective tissue of the extracellular matrix (ecm) in the vicinity of collagen fibers (C) and few small mitochondria (mt). **(TEM X 12,000).** **(F)** Regular pattern of Z-lines in between myocyte edges (arrow heads) surrounded by myofibrils (M) with regular rows of oval mitochondria (mt) in-between. Collagen fibers (C) is laid in the extracellular matrix (ecm) near a blood vessel (bv). Two nuclei (N); one of them is seahorse shape with prominent nucleolus (arrow), extended and peripherally condensed chromatin (ch) giving the morphological appearance of a macrophage. **(TEM X 12,000).**

intercalated disc in-between myocytes with a step-like pattern connected by Z lines, regular rows of mitochondria were revealed. A TC like cell with elongated nucleus and dark peripheral chromatin, cell membrane and blood vessels were evident (Fig. 4. panel E). TC with elongated nucleus and peripherally condensed chromatin surrounded by a narrow cytoplasmic rim was seen. Collagen deposition in the extra-cellular matrix with telopodes were visible. A nearby row of elongated mitochondria, cardiac myofibrils connected by Z-lines were clearly seen (Fig. 4. panel F). In group II, which was treated with HCQ, the TEM images revealed irregularly arranged cardiac myofibrils bisected by Z lines with focal areas of fragmentation. The nucleus of cardio myocytes was irregular with extended chromatin surrounded by swollen mitochondria. Moreover, there was leucocytic cellular infiltration with irregular nuclei in the vicinity of neighboring blood vessels (Fig. 5. panel A). The even arrangement of myofibrils showed a bamboo shape with dark Z-lines between myocytes was damaged, and vacuoles and curv-circular bodies aggregates were seen in-between. The mitochondria were dilated and compact, with an uneven shape and organization. In group II, which received HCQ treatment, irregularly arranged cardiac myofibrils bisected by Z lines were observed, along with focal areas of fragmentation and an irregular nucleus of the cardio-myocyte surrounded by swollen mitochondria. Leucocytic cellular infiltration with irregular nuclei was evident in the vicinity of neighboring blood vessels. The even arrangement of myofibrils showing a bamboo shape with dark Z-lines between myocytes was damaged and vacuoles and curv-circular body aggregates were seen in-between. Dilated and compact mitochondria with uneven shape and organization were also observed (Fig. 5. panel B). Furthermore, disorganized cardiac myofibrils with dark Z-lines between myocytes and areas of degeneration with irregular rows of mitochondria of variable sizes and tubular packed prominent cristae inside were evident in group II (Fig. 5. panel C). The nucleus of the TC was seen in a division state with two nucleoli and condensed peripherally situated chromatin. Telopodes were seen arising from the TC extremities, and collagen deposition in the extracellular matrix separated myofibrils with dark Z-lines between sarcomere edges, and few mitochondria were also clear (Fig. 5. panel D). Accumulation of interstitial fluid, loss of regular arrangement of myofibrils with Z-lines in-between and degenerated areas and swollen circular mitochondria; some of which are vacuolated were clearly seen (Fig. 5. panel E). Fragmentation and loss of regular arrangement of myofibrils with vacuoles and Z-lines in-between were evident. Irregular shrunken nucleus with prominent nucleolus near a blood vessel was noticed (Fig. 5. panel F). Group III, which received Zn treatment, showed a regular

arrangement of muscle fibers with normal striations and Z-lines in between. Normally arranged rows of oval mitochondria and elongated nucleus of the interstitium, most commonly TC with peripherally condensed chromatin and long processes or telopodes were seen. Extracellular collagen was noticed between TC and cardiac myofibrils, and cardiac myocytes with oval nuclei, which exhibited extended chromatin and Z-lines between cardio-myocyte edges, and rows of oval mitochondria in-between cardio-myocytes were clearly observed (Fig. 6 panel A&B). Cardiac myofibrils with a regular arrangement of myofilaments linked by Z-lines, regular rows of mitochondria parallel to the myofibrils, and sarcoplasmic reticulum visible between mitochondria and the external lamina (Fig. 6. panel C). Z-lines between the edges of cardio myocytes with regular rows of rectangular mitochondria laid in between, ending at the intercalated disc region and t-tubules were noticed (Fig. 6. panel D). Cardio-myocyte progenitor cell (CMP) with elongated nucleus showed peripherally condensed beaded chromatin and small developing Golgi and vesicles were noticeable. Cardio-myocyte fibrils were connected by Z-lines with rows of elongated mitochondria in-between. Basal lamina of cardio-myocytes enclosed the CMP cell wall. Poorly differentiated desmosome and reduced electron-dense collagen material in a gap between contacting membranes of CMP and cardio-myocytes was shown (Fig. 6. panel E). Elongated nucleus of a TC present in a loose extracellular matrix with prominent nucleolus and peripherally condensed chromatin was seen. Tc also exhibited telopode and smooth endoplasmic reticulum and was separated from cardio-myocytes by cardiac external lamina and loose extracellular matrix. Cardio-myocytes were connected by Z-lines with regular rows of mitochondria in-between (Fig. 6. panel F). The TEM images of group IV (Zn and HCQ co-treatment) showed intact cardiac myofibrils with swollen mitochondria, vacuolated sarcoplasm with intact rows of intercalated discs. Noticed classic Z-band between cardio-myocyte edges. An elongated nucleus of a TC with telopode was visible (Fig. 7. panel A). Other micrograph exhibited regular arrangement of myofilaments, some of which were vacuolated connected by Z-lines. Integral intercalated discs of step-like design were visible. Two elongated nuclei of CSC located in a loose extracellular matrix with peripherally condensed chromatin were captured. The CSC of typical leptofibrils was closely supported by Tc processes. Extracellular collagen was laid next to them (Fig. 7. panel B). Other image revealed regular arrangement of myofilaments connected by Z-lines and integral intercalated discs with a step-like design. Two cardiac stem cells located near a blood vessel with two large dented nuclei, fewer dispersed chromatin, and prominent nucleoli were noticed. Endoplasmic reticulum, collec-

Table 1A
Statistical analysis of serum level of CK-MB:

	Group I	Group II	Group III	Group IV	F test	P value
CK-MB (U/L)	22.00 ± 4.92	2070.9 ± 223.49	24.0 ± 5.19	895.0 ± n 100.14	627.036	0.001*
P 1		0.001*	0.998	0.001*		

* Significant p value < 0.05.

P 1: Comparison with Group I.

Table 1B
Statistical analysis of serum level of troponin (cTnI):

	Group I	Group II	Group III	Group IV	F test	P value
Troponin (cTnI) (ng/mL)	0.10 ± 0.02	0.30 ± 0.07	0.10 ± 0.03	0.11 ± 0.03	61.339	0.110
P 1		0.001*	0.998	0.971		

* Significant p value < 0.05.

P 1: Comparison with Group I.

Table 1C
Percentage area of CD117 immuno-staining.

	Group I	Group II	Group III	Group IV	F test	P value
Area (%)	2.015 ± 0.135	8.312 ± 1.457	3.356 ± 0.793	3.251 ± 0.774	46.081	0.001*
P 1		0.001*	0.034*	0.049*		

* Significant p value < 0.05.

P 1: Comparing the last three groups to the control one (Group I).
Standard deviation (SD) is expressed in ±.

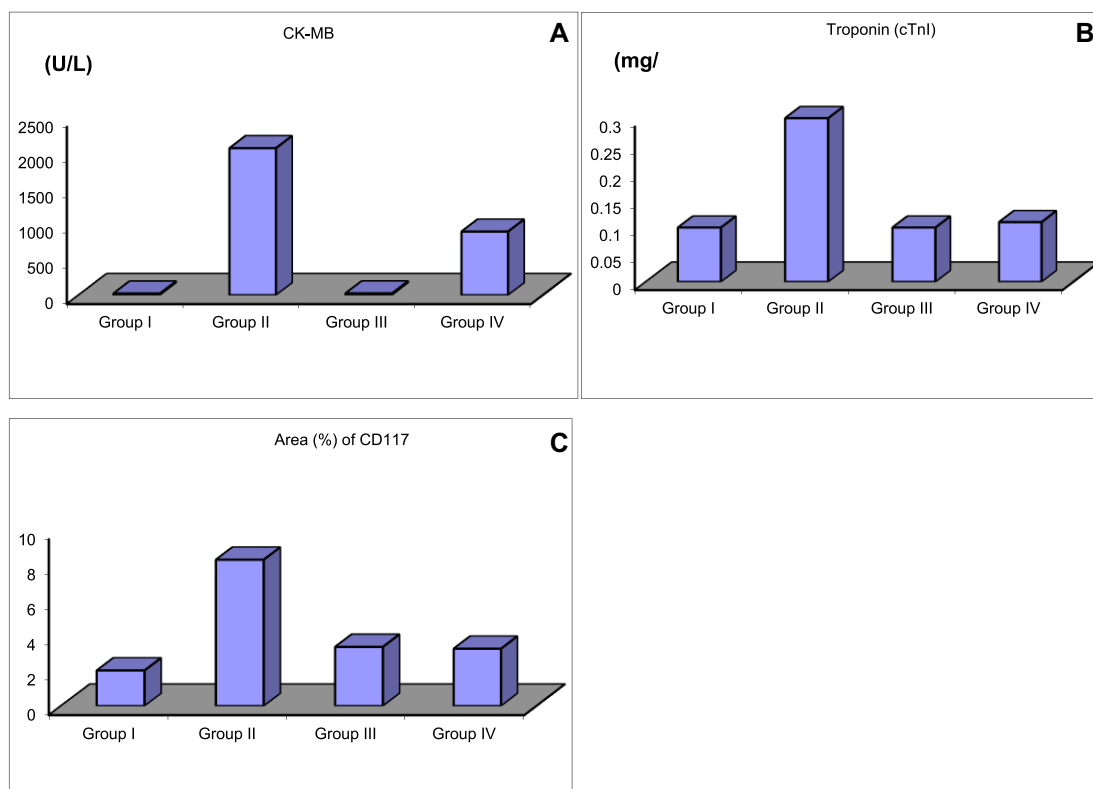


Fig. 8. Histograms: 8.A. troponin (cTnI) in mg/ml. 8. B. CK-MB in U/L. 8.C. Percentage area of CD117 immuno-staining.

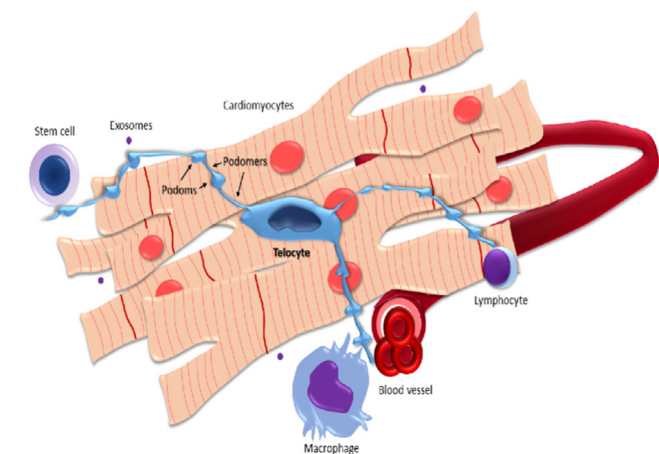


Diagram 1. The typical morphology of a telocyte (TC) with long cytoplasmic projections, or telopodes, demonstrating alternating podomers and podoms making contacts with cardiomyocytes and interstitial components (such as immune cells, blood vessels, etc.). After Klein et al. (2021).

tions of minor and clear vacuoles creating a multi-locular look, scarce condensed granules, and lysosomes were seen. Extracellular collagen was laid between cell outlines and cardiac myofibrils (Fig. 7. panel C). This micrograph displayed typical TCs with elongated nuclei which contained heterochromatin in their periphery and prominent nucleoli. Their cytoplasm contained small mitochondria and vesicles in the podoms. The TCs were located near cardiomyocytes that are connected by Z-lines with regular rows of mitochondria arranged in between (Fig. 7. panel D). A magnified photomicrograph of the previous one showed typical TCs with elongated nuclei with peripherally condensed chromatin giving a beaded appearance and various outbuilding extracellular vesicles from the podoms in the connective tissue of the extracellular matrix in the locality of collagen fibers and few small mitochondria (Fig. 7. panel E). Regular pattern of Z-lines in between myocyte edges surrounded by myofilaments with regular rows of oval mitochondria in-between were captured. Collagen fibers was laid in the extracellular matrix near a blood vessel. Two nuclei; one of them is seahorse shape with prominent nucleolus, extended and peripherally condensed chromatin giving the morphological appearance of a macrophage were visible (Fig. 7. panel F).

3.3. Statistical analysis

3.3.1. Cardiac enzymes statistical level in the four studied groups:

The myocardial parameters including CK-MB were significantly elevated in the HCQ-treated (group II) and HCQ and Zn-treated (group IV) groups in comparison to the control one (group I) (Table 1.A and Fig. 8.A).

While cardiac Troponin (cTnI) was significantly elevated in HCQ-treated (group II) rats as compared to the control group (group I) only (Table 1.B and Fig. 8.B).

3.3.2. Percentage area of CD117 immuno-staining in cardio-myocytes of the four experimental groups:

See Table 1.C and Fig. 8.

4. Discussion

The COVID-19 pandemic initiated by SARS-CoV-2 has been the most significant health crisis of this century, resulting in a surge of illness and death worldwide. The virus has been linked to an increased risk of developing various pathologies, particularly those affecting the cardiovascular system, which are commonly associated with oxidative stress and lipid imbalances (Magadum & Raj-Kishore, 2020). Our study aimed to investigate the protective role of Zinc against HCQ-induced cardiomyopathy. We measured serum levels of cardiac enzymes and conducted a widespread histopathological examination of the heart, which was supported by statistical analysis. Our findings suggest that treatment modifications play a crucial role in avoiding such complications. In our study, we found that the myocardial biochemical parameters profile of CK-MB was significantly elevated in the HCQ-treated group and the HCQ and Zinc-treated group, compared to the control group. Additionally, troponin I (cTnI) ranks were significantly elevated in the HCQ-treated rats (group II) paralleled to the control group. Our findings are consistent with El Shishtawy et al., 2015 and Muller (2021), who reported that elevated cardiac markers may be associated with severe erosion and necrosis of the myocardium. Bertinchant et al., 2003 also noted that cardiac troponin (cTnI) is a highly sensitive and specific marker of myocardial cell damage.

The histopathological study confirmed the diagnostic significance of troponin (cTnI) in our rat model of HCQ-induced cardiomyopathy. Tselios et al., 2019 suggested that cardiac biomarkers should be evaluated as a screening assessment for prolonged treatment with 4-aminoquinoline (4-AQ). In case of any abnormality, an *endo*-myocardial biopsy may be necessary to confirm the diagnosis of 4-AQ toxicity. According to Hartupepe et al., 2017, inflammation plays a significant role in the remodeling process of inflammation-induced remodeling in an experimental model. In our study, light microscopy of rat myocardium from the HCQ-treated group revealed myocytes with profoundly eosinophilic cytoplasm, widened blood capillaries, zones of hemorrhage, and extravasated blood. We also detected crucial zones of damage and cytolysis of myocytes, hydrophobic changes of myofibrillar structure with striations, branched look and discontinuity with contiguous myofibrils, widespread cellular leukocyte infiltration, edema, and a wavy organization of some muscle fibers. Fibroblast-like cells with elongated nuclei were also seen. In addition, the cardiac myocytes of the HCQ-treated group displayed myofibrillar structure with vacuolations and pyknotic nuclei. These histopathological changes are consistent with previous studies that confirmed the success of the HCQ-treated rat model ((Louch et al., 2004; Vilahur et al., 2011; Kannan & Quine, 2013). The co-administration of HCQ and Zn in group IV resulted in the observation of cardiac myofibrils with normal striations and oval nuclei, along with the presence of fibroblast-like cells with elongated

nuclei, which is consistent with the findings of previous studies by Powell, 2000; Karagulova et al., 2007 and Xu et al., 2014, indicating the importance of Zn in cellular functions and organization. Imbalances in Zn levels have been linked to the pathogenesis of several cardiovascular disorders. Research has shown that intracellular Zn levels were reduced in rat hearts exposed to ischemia/reperfusion, and that Zn supplementation may protect the heart, suggesting that maintaining Zn homeostasis is crucial for cardiac survival during reperfusion. The C-kit protein (CD117) is a type III tyrosine-protein kinase that recognizes the stem cell factor (SCF) ligand. Through growth, the C-kit receptor is expressed in cardiac progenitors of cardio-myogenesis and in others with different developmental patterns. This receptor-ligand interface triggers signaling pathways of cellular proliferation, growth, and differentiation. Previous studies have shown that C-kit is significant in epicardial, mesothelial, and sub-epicardial stromal cells, which may indicate the presence of a stem/progenitor niche and *trans*-differentiation procedures (Iancu et al., 2019). In our study, CD117 immunohistochemical staining showed a statistically significant increase in CD + v reaction in HCQ-treated rat hearts (group II), Zn-treated group (III) and group IV compared to the control group. Thus, inhibiting myocyte cell death and promoting the generation of new ones may represent significant targets in human heart failure therapy. Recent evidence of myocardial renewal enhancement has revealed cells called TCs, previously referred to as interstitial Cajal-like cells, which are thought to stimulate endogenous and exogenous stem cells (CSC) and support the immigration of progenitor cells to damaged myocardium (Kostin, 2016). In our study, we utilized CD117 immuno-histochemical staining and quantified the CD117 (+) areas using an image analyzer in all groups. This approach is supported by Cretoiu and Popescu (2014), who suggested that double immune labeling for C-kit/CD117 could be useful in identifying (TCs) from other stromal cells by light microscopy. Additionally, Kajstura et al., 2010 highlighted the importance of C-kit in visualizing TCs and studying their role in normal and pathological states. In our study, we observed CD117 (+) mast cells in the cardiac myocyte sections of the HCQ and Zn-treated group, located in the vicinity of regenerated myocardial bundles, with (TCs) displaying telopodes giving a starry sky look. Furthermore, we detected CD117 (+) immunoreactivity in blood vascular endothelium and between recovered cardiac muscle fibers, which aligns with Legere et al., 2019 who emphasized the presence of mast cells in heart tissue adjacent to myocardial remodeling and suggested that they are a valuable target for therapeutic intervention following cardiac injury. Zhou et al., 2010 suggested that a large number of CD117 (+) cells in the human heart were mast cells and that the recently reported CD117 (+) putative cardiac progenitor stem cells were actually mast cells. Consistent with Cove-Smith et al., 2014, we observed wavy vacuolated myofibrils connected by Z-lines and oval nuclei surrounded by clear spaces in semi-thin sections of cardio myocytes of HCQ treated rats, along with congested blood vessels. TCs were observed as diverged spindle, triangular, or cubical cells with elongated processes (telopodes) rising from the cell body, displaying homocellular connection with another TC's telopodes and heterocellular connections between (TCs) and cardio myocytes, along with multi-vesicular bodies. TCs and their telopodes were situated close to cardio myocytes, blood capillaries, and nerve endings and were anticipated to function as mechanoreceptors/transducers according to Gherghiceanu and Popescu, 2010 and Abdel Gawad et al., 2020. CSC progenitors and TCs were found to undergo continuous cardiac regeneration, with TCs being able to form connection plaques with the extracellular matrix due to their elongated telopodes (Fausone-Pellegrini and Bani, 2010). According to Cucu et al., 2022 TCs were also found in cardiac stem cell (CSC) niches, where it appears that they help with cardiac renewal and regeneration.

Because of the cellular prolongations' ultrastructural characteristics, they were given the name "TCs." Their extensions, known as telopodes, are typically found in an alternation of thin segments (called podomers) and dilated segments (called podoms). The trio of organelles known as "calcium uptake/releasing units"—mitochondria, endoplasmic reticulum, and caveolae—are housed in podosomes.

Regarding ultrastructural findings, the sarcoplasm of HCQ-treated myocytes exhibited cardiac myofibrils with areas of degeneration, irregular shrunken nucleus, swollen vacuolated mitochondria, and phagocytic cellular infiltrate near a blood vessel (Goyal et al., 2015). Fragmentation and loss of regular organization of myofibrils with vacuoles were also evident, as well as the accumulation of interstitial fluid and dark Z-lines between myocytes. These observations align with previous studies suggesting that chronic HCQ therapy may lead to cardiomyopathy with wall thickening and microscopic organizational alterations. Specifically, cardiomyopathy exhibits an expansion and vacuolization of cardiac myocytes with curvilinear body aggregates (Tonnesmann et al., 2013). Cardiac fibrosis and inflammation were also present in the HCQ-treated group, which agrees with previous studies of Beliveau et al., 2015; Huet et al., 2015 and Aboulhoda, 2017 indicating that myocardial fibrosis is accompanied by collagen accumulation and cardiomyopathies. Changes in the ultramicroscopic structure, such as loss of T-tubules and alterations of the extracellular matrix, have also been observed in myocardial injury. Additionally, the increase of myo-fibroblasts with the enhancement of fibrosis has been reported. Electron microscopic examination revealed that TCs play a vital role in cardiovascular restoration and cardiac healing, as they are in contact with young cardiomyoblasts. TCs appeared as forked spindle, triangular, or cubical cells with long processes (telopodes) that connect with other TCs and cardio myocytes. Vesicular bodies were also detected in telopodes. These findings support the hypothesis that TCs and their telopodes may regulate and host the myocardial originators (CSC progenitor cells), contributing to cardiovascular renewal and repair (Petre et al., 2016). According to Gupta et al. 2016, the effect of CQ on restoration after myocardial infarction may not directly affect cardio myocytes but rather have a more significant impact on other cardiac cells such as fibroblasts. Cardiac fibroblasts can transform into myo fibroblasts, which have increased proliferation and secretion capabilities, and CQ can reduce their migration and contractility. Navarro-Hortal et al., 2019 and Tarazón et al., 2022 found that changes in cardiac tissue morphology after myocardial infarction may be related to alterations in mitochondrial ultrastructure, which are essential for maintaining cellular homeostasis and proper function. Zn was shown to play a dynamic role in protecting cells against oxidative damage, which is consistent with the regular arrangement of myofilaments and intact intercalated discs observed in the ultrastructure study of group IV cardio myocytes. The TEM study also revealed the capacity of putative cardiac stem cells to self-renew and produce differentiated cardio myocyte progenitors, which was improved by Zn supplementation in groups III and IV. Popescu et al., 2009 and Ellison et al., 2010 demonstrated different stages of development of cardiac progenitor cells and suggested that CSC progenitors and interstitial cells sustain a continuous cardiac replenishment process in the adult mammalian heart. In our study, regular patterns of Z-lines, myofilaments, and mitochondria were observed in between cardio myocyte edges, with collagen fibers in the extracellular matrix near a blood vessel. The presence of seahorse-shaped nuclei with prominent nucleoli and peripherally condensed chromatin suggested macrophages, which are known to assist in phagocytosis, dead cell scavenging, and cytokine and growth factor release to enhance the restorative process. Lafuse et al. 2021 reported that monocytes quickly accumulated in the heart after ischemic damage and differentiated into

engaged macrophages, which reinforced inflammation by secreting pro-inflammatory cytokines and chemokines, and matrix metallo-proteinase. Hulsmans et al., 2016 and Frangogiannis (2019) emphasized that the heart is a heterogeneous organ that contains various types of cells, including cardio myocytes, fibroblasts, pericytes, smooth muscle cells, endothelial cells, and different varieties of immune cells.

5. Conclusion:

It is advisable to use CQ/HCQ with caution, keeping in mind the dosage and duration of therapy, and avoiding combination with other medications known to cause harmful effects on the heart. Our findings suggest that Zn may have a protective effect against HCQ-induced cardiotoxicity. Patients receiving long-term HCQ treatment should undergo regular evaluation of their cardiac enzyme levels and echocardiogram to monitor any potential cardiac damage.

Availability of data and materials:

All the data has been added to this article.

Consent for publication:

The undersigned, on behalf of the listed authors give my consent for the publication of identifiable details to be published in the above Journal and Article.

Aim of the work

This research was planned to study defensive role of Zn alongside the injurious side effects of HCQ on the heart of male experimental animals Physiologically, ultra-structurally, and enzymatically.

Ethical Approval and Consent to participate

Ethical Committee of Animal Researches of Ajman university has approved the work under the number (P-H-F-Jun-16).

Funding

This Article was supported by Ajman University Internal Research Grant No. 2021-IRG-PH-3. The research findings presented in this Article are solely the authors responsibility.

Declaration of Competing Interest

The authors declare that they have no known competing financial interests or personal relationships that could have appeared to influence the work reported in this paper.

References

- Abdallah, S., Mhalla, Y., Trabelsi, I., Sekma, A., et al., 2023. Twice-Daily Oral Zinc in the Treatment of Patients with Coronavirus Disease 2019: A Randomized Double-Blind Controlled Trial. *Clinical Infectious Diseases* 76 (2), 185–191. <https://doi.org/10.1093/cid/ciac807>. PMID:36367144.
- Abdel-Gawad, S., Al-Shahed, F., Abd El-Zaher, M., 2020. Histological and immunohistochemical study of telocytes in the heart of male albino rats in different age groups. *The Scientific Journal of Al-Azhar Medical Faculty, Girls, a publication of Scientific Society of Al Azhar Faculty of Medicine (Girls)* 4 (3), 373–382. https://doi.org/10.4103/sjamf.sjamf_43_20.

- Aboulhoda, B.E., 2017. (2017): Age-related remodeling of the JAK/STAT/SOCS signaling pathway and associated myocardial changes: From histological to molecular level. *Ann. Anat.* 214, 21–30. <https://doi.org/10.1016/j.aanat.2017.07.003>.
- Anakwue, R.C. & Otamiri, C. 2018. Petroleum Products Induced- Cardiac Enzymes and Histological Changes in Wistar Rat Model: Is there any Implications for Cardiovascular Disease in Nigeria? *Annals of Medical and Health Sciences Research*. ISSN: Print -2141-9248, Online - 2277-9205.
- Babaei, H., Razmarai, N., Assadnassab, G., Mohajjel Nayebi, A., Azarmi, Y., Mohammadnejad, D., et al., 2020. Ultrastructural and echocardiographic assessment of chronic doxorubicin-induced cardiotoxicity in rats. *Arch. Razi Inst.* 75, 55–62. <https://doi.org/10.22092/ari.2019.116862.1177>. PMID:32292003.
- Bancroft, J.D., Gamble, M., 2008. *Theory and Practice of Histological Techniques*. Churchill Livingstone, Elsevier, China, p. 633.
- Bastway, M., Hasona, N.A., Abdel Hamid, H., 2008. Effects of Zinc Acetate on Thioacetamide-Induced Hepatotoxicity in Rats. *Bull. Egypt. Soc. Physiol. Sciences* 28 (2), 81–90. <https://doi.org/10.21608/BESPS.2008.37034>.
- Beliveau, P., Cherié, F., Anderson, S.A., Taylor, J.L., Arai, A.E., Hsu, L.-Y., 2015. Quantitative assessment of myocardial fibrosis in an age-related rat model by ex vivo late gadolinium enhancement magnetic resonance imaging with histopathological correlation. *Comput. Biol. Med.* 2015 (65), 103–113. <https://doi.org/10.1016/j.combiomed.2015.07.027>.
- Bertinchant, J.P., Polge, A., Juan, J.M., Oliva-Lauraire, M.C., Giuliani, I., et al., 2003. Evaluation of cardiac troponin I and T levels as markers of myocardial damage in doxorubicin-induced cardiomyopathy rats, and their relationship with echocardiographic and histological findings. *Clin. Chim. Acta.* 329 (1–2), 39–51. [https://doi.org/10.1016/s0009-8981\(03\)00013-5](https://doi.org/10.1016/s0009-8981(03)00013-5).
- Collins, H.E., Kane, M.S., Litovsky, S.H., et al., 2021. *Front. Aging* 2 (2021), 06. <https://doi.org/10.3389/frag.2021.670267>.
- Costedoat-Chalumeau, N., Hulot, J.S., Amoura, Z., et al., 2007. (2007): Cardiomyopathy related to antimalarial therapy with illustrative case report. *Cardiology* 107, 73–80. <https://doi.org/10.1159/000094079>.
- Cove-Smith, L., Woodhouse, N., Hargreaves, A., Kirk, J., Smith, S., Price, S.A., et al., 2014. (2014): An integrated characterization of serological, pathological, and functional events in doxorubicin-induced cardiotoxicity. *Toxicol. Sci.* 140, 3–15. <https://doi.org/10.1093/toxsci/kfu057>.
- Cretoi, S.M., Popescu, L.M., 2014. Telocytes revisited. *Biomol. Concepts* 5, 353–369. <https://doi.org/10.1159/000497194>. Epub 2019 Mar 15. Doi: 10.1515/bmc-2014-0029.
- Cucu, I., Nicolescu, M., Busnatu, S.S., Manole, C., 2022. Dynamic Involvement of Telocytes in Modulating Multiple Signaling Pathways in Cardiac Cytoarchitecture. *Int. J. Mol. Sci.* 23 (10), 5769. <https://doi.org/10.3390/ijms23105769>. doi: 10.1369/ijhc.2009.955146. Epub 2009 Dec 21.
- Elgharabawy, R., El Sayed, I., Rezk, N., Tousson, E., 2021. Therapeutic Impact of Costus (Sausurea lappa) Against Ehrlich Solid Tumor-Induced Cardiac Toxicity and DNA Damage in Female Mice. *Front. Pharmacol.* 2021, (12). <https://doi.org/10.3389/fphar.2021.708785>.
- Ellison, G.M., Galuppo, V., Vicinanza, C., et al., 2010. (2010): Cardiac stem and progenitor cell identification: different markers for the same cell? *Front. Biosci.* 2, 641–652. <https://doi.org/10.2741/s91>.
- Elshishtawy, M.A., Hassan, K.H., Ramzy, R., Berri, F., et al., 2015. Comparative toxicity study of chloroquine and hydroxychloroquine on adult albino rats. *European Scientific Journal February 2015 / SPECIAL/ Edition Vol 1*.
- Ezeiruaku, F.C. 2019. Cardiac Markers: An Index in the Assessment of Cardiovascular Disease in Diabetic Patients in Bayelsa State, Niger Delta Region, South of Nigeria. *Journal of Diabetes Mellitus* 9 4, 153–166. <https://doi.org/10.4236/jdm.2019.94015>.
- Fausson-Pellegrini, M.S., Bani, D., 2010. Relationships between telocytes and cardio-myocytes during pre- and post-natal life. *J. Cell Mol. Med.* 14 (5), 1061–1063. <https://doi.org/10.1111/j.158204934.2010.01074.x>.
- Frangogiannis, N.G., 2019. Cardiac fibrosis: Cell biological mechanisms, molecular pathways and therapeutic opportunities. *Mol. Asp. Med.* 65, 70–99. <https://doi.org/10.1016/j.mam.2018.07.001>.
- Gherghiceanu, M., Popescu, L.M., 2010. Cardio myocyte precursors and telocytes in epicardial stem cell niche: electron microscope images. *Journal of cellular and molecular medicine.* 14 (4), 871–877. <https://doi.org/10.1111/j.1582-4934.2010.01060.x>.
- Golomb, E., Matza, D., Cummings, C., Schwab, H., Kodavanti, U., Schneider, A., et al., 2012. myocardial mitochondrial injury induced by pulmonary exposure to particulate matter in rats. *Toxicologic pathology* 40, 779–788. <https://doi.org/10.1177/0192623312441409>.
- Goyal, S.N., Sharma, C., Mahajan, U.B., Patil, C.R., Agrawal, Y.O., Kumari, S., Arya, D.S., Ojha, S., 2015. Protective Effects of Cardamom in Isoproterenol Induced Myocardial Infarction in Rats *Int. J. Mol. Sci.* 16 (11), 27457–27469. <https://doi.org/10.3390/ijms161126040>.
- Gupta, S.S., Zeglinski, M.R., Rattan, S.G., Landry, N.M., Ghavami, S., Wigle, J.T., 2016. Inhibition of autophagy inhibits the conversion of cardiac fibroblasts to cardiac myofibroblasts. *Oncotarget.* 2016 (7), 78516–78531. <https://doi.org/10.18632/oncotarget.12392>.
- Hartupée, J., Szalai, G.D., Wang, W., Ma, X., Diwan, A., Mann, D.L., 2017. Impaired protein quality control during left ventricular remodeling in mice with cardiac restricted overexpression of tumor necrosis factor. *Circ. Heart Fail.* 2017, 10. <https://doi.org/10.1161/circheartfailure.117.004252>.
- Hsieh, C.C., Li, C.Y., Hsu, C.H., Chen, H.L., Chen, Y.H., Liu, Y.P., et al., 2019. Mitochondrial protection by simvastatin against angiotensin II-mediated heart failure. *Br. J. Pharmacol.* 176, 3791–3804. <https://doi.org/10.1111/bph.14781>.
- Huet, E., Gabison, E., Vallee, B., Mougnot, N., Linguet, G., Riou, B., Jarosz, C., Menashi, S., Besse, S., 2015. Deletion of extracellular matrix metalloproteinase inducer/CD147 induces altered cardiac extracellular matrix remodeling in aging mice. *J. Physiol. Pharmacol. Off. J. Pol. Physiol. Soc.* 2015 (66), 355–366.
- Hulsmans, M., Sam, F., Nahrendorf, M., 2016. (2016): Monocyte and macrophage contributions to cardiac remodeling. *J. Mol. Cell. Cardiol.* 93, 149–155. <https://doi.org/10.1016/j.yjmcc.2015.11.015>.
- Iancu, C.B., Rusu, M.C., Mogoantă, L., Hostiu, S., Grigoriu, M., 2018. Myocardial Telocyte-Like Cells: A Review Including New Evidence. *Cells Tissues Organs.* 206 (1–2), 16–25. <https://doi.org/10.1159/000497194>.
- Iancu, C.B., Rusu, M.C., Mogoanta, L., Hostiu, S., Toader, O.D., 2019. The Telocytes in the Subepicardial Niche. *Appl. Sci.* 9 (8), 1615. <https://doi.org/10.3390/app9081615>.
- Ibrahim, N., Elmorsheddy, K., Radwan, D., Buabeid, M., 2021. The impact of oral ciprofloxacin on the structure and functions of rat gastric mucosa. *Saudi j. of biological sciences.* 29 (4), 2187–2198. <https://doi.org/10.1016/j.sjbs.2021.11.042>.
- Joyce, E., Fabre, A., Mahon, N., 2013. Hydroxychloroquine cardiotoxicity presenting as a rapidly evolving biventricular cardiomyopathy: key diagnostic features and literature review. *European Heart Journal: Acute Cardiovascular Care* 2 (1), 77–83. <https://doi.org/10.1177/2048872612471215>.
- Kajstura, J., Gurusamy, N., Ogórek, B., Goichberg, P., 2010. Myocyte turnover in the aging human heart. *Circ. Res.* 2010 (107), 1374–1386. <https://doi.org/10.1161/CIRCRESAHA.110.231498>.
- Kamp, T.J., Hamdan, M.H., January, C.T., 2020. Chloroquine or Hydroxychloroquine for COVID-19: Is Cardiotoxicity a Concern? *Journal of the American Heart Association.* 9 (12), e016887.
- Kannan, M.M., Quine, S.D., 2013. Ellagic acid inhibits cardiac arrhythmias, hypertrophy and hyperlipidaemia during myocardial infarction in rats. *Metabolism* 2013 (62), 52–61. <https://doi.org/10.1016/j.metabol.2012.06.003>.
- Karagulo, G., Yue, Y., Moreyra, A., Boutjdir, M., Korichneva, I., 2007. Protective role of intracellular zinc in myocardial ischemia/reperfusion is associated with preservation of protein kinase C isoforms. *J. Pharmacol. Exp. Ther.* 2007 (321), 517–525. <https://doi.org/10.1124/jpet.107.119644>.
- Klein, M., Csöbőnyeiová, M., Žiaran, S., Danišovič, L., Varga, I., 2021. Cardiac Telocytes 16 Years on-What Have We Learned So Far, and How Close Are We to Routine Application of the Knowledge in Cardiovascular Regenerative Medicine? *Int J Mol Sci.* 22 (20), 10942. <https://doi.org/10.3390/ijms222010942>.
- Kostin, S., 2016. Cardiac telocytes in normal and diseased hearts. *Seminars in Cell & Developmental Biology.* 55, 22–30. <https://doi.org/10.1016/j.semcdb.2016.02.023>.
- Lafuse, W., Wozniak, D., Rajaram, M., 2021. Role of Cardiac Macrophages on Cardiac Inflammation, Fibrosis and Tissue Repair. *Cells.* 10 (1), 51. <https://doi.org/10.3390/10.3390/cells10010051>.
- Legere, S., Haidl, I., Légaré, J., JandMarshall, J., 2019. Mast Cells in Cardiac Fibrosis: New Insights Suggest Opportunities for Intervention. *Front. Immunol.* 28 March 2019. *Sec. Inflammation.* <https://doi.org/10.3389/fimmu.2019.00580>.
- Louch, W.E., Bito, V., Heinzl, F.R., Macianskiene, R., Vanhaecke, J., Flameng, W., 2004. Reduced synchrony of Ca²⁺ release with loss of T-tubules—a comparison to Ca²⁺ release in human failing cardio-myocytes. *Cardiovasc. Res.* 2004 (62), 63–73.
- Magadam, A., Raj Kishore, R., 2020. Cardiovascular Manifestations of COVID-19 Infection. *Cells.* 9 (11), 2508. <https://doi.org/10.3390/cells9112508>.
- MSDS (Material Safety Data Sheet) 2011. Hydroxychloroquine sulfate, Toxicological Information. Product Number: H0915, CAS-No. 747-36-4, EC-No. 212-019-3. Sigma-Aldrich, 3050 Spruce Street, Saint Louis, MO 63103, USA, pp:1-5.
- Mubagwa, K., 2020. Cardiac effects and toxicity of chloroquine: a short update. *Int. J. Antimicrob. Agents.* 56, (2). <https://doi.org/10.1016/j.ijantimicag.2020.106057>. Published online 2020 106057.
- Muller, R., 2021. Systemic toxicity of chloroquine and hydroxychloroquine: prevalence, mechanisms, risk factors, prognostic and screening possibilities. *Rheumatology. International* 41, 1189–1202. <https://doi.org/10.1007/s00296-021-04868-6>.
- Muthukrishnan, P., Roukoz, H., Grafton, G., Jessurun, J., Colvin-Adams, M., 2011. Hydroxychloroquine-Induced Cardiomyopathy. *Circulation. Heart Failure.* 2011 (4), e7–e8. <https://doi.org/10.1161/CIRCHEARTFAILURE.110.959916>.
- Naddaf, E., Paul, P., Omar, F., Ezzeddine, A., 2021. Chloroquine and Hydroxychloroquine Myopathy: Clinical Spectrum and Treatment Outcomes. *Frontiers in Neurology.* 11. <https://doi.org/10.3389/fneur.2020.616075>.
- Navarro-Hortal, M., Ramirez-Tortosa, C., Quidés, J., et al., 2019. Heart Histopathology and Mitochondrial Ultrastructure in Aged Rats Fed for 24 Months on Different Unsaturated Fats (Virgin Olive Oil, Sunflower Oil or Fish Oil) and Affected by Different Longevity. *Nutrients.* 11 (10), 2390. <https://doi.org/10.3390/nut1102390>.
- Nour, M., Sarhan, N., Mazroa, S., Gawish, S., 2017. Histological and immunohistochemical study of cardiac telocytes in a rat model of isoproterenol-induced myocardial infarction with a reference to the effect of grape seed extract. *Acta Histochemica* 119 (7). <https://doi.org/10.1016/j.acthis.2017.09.007>.
- Pasadhika, S., Fishman, G.A., 2010. Effects of chronic exposure to hydroxychloroquine or chloroquine on inner retinal structures. *Eye (Lond)* 24 (2), 340–346. <https://doi.org/10.1038/eye.2009.65>.

- Petre, N., Rusu, M.C., Pop, F., Jianu, A.M., 2016. Telocytes of the mammary gland stroma. *Folia Morphologica* 2016 (75), 224–231. <https://doi.org/10.5603/FM.a2015.0123>.
- Pogodina, L.S., Shornikova, M.V., Chentsov, Y.S., 2006. Electron Microscopy Description of Cardio-myocytes from the Left Ventricle of Rat Heart after Apoptosis Induction by Isoproterenol. *Biology Bulletin* 33 (1), 19–29. <https://doi.org/10.1134/S1062359006010031>.
- Popescu, L.M., Gherghiceanu, M., Manole, C.G., et al., 2009. (2009): Cardiac renewing: interstitial Cajal-like cells nurse cardio-myocyte progenitors in epicardial stem cell niches. *J. Cell. Mol. Med.* 13, 866–886. <https://doi.org/10.1111/j.1582-4934.2009.00758.x>.
- Powell, S.R., 2000. The antioxidant properties of zinc. *J. Nutr.* 2000 (130), 1447S–1454S. <https://doi.org/10.1093/jn/130.5.1447S>.
- Rusu, M., Pop, F., Hostiu, S., Curca, G.C., Jianu, A.M., Paduraru, D., 2012. Telocytes form networks in normal cardiac tissues. *Histol. Histopathol.* 27 (6), 807–816. <https://doi.org/10.14670/HH-27.807>.
- Suvarna, S.K., Layton, C., Bancroft, J.D., 2018. *Bancroft's theory and practice of histological techniques*. Philadelphia Churchill Living Stone, pp. 78–80.
- Taherian, E., Rao, A., Malemud, C.J., Askari, A.D., 2013. The biological and clinical activity of antimalarial drugs in autoimmune disorders. *Curr. Rheumatol. Rev* 9, 45–62. <https://doi.org/10.2174/1573397111309010010>.
- Tarazón, E., Pérez-Carrillo, L., Portolés, M., Roselló-Lletí, E., 2022. Electron Microscopy Reveals Evidence of Perinuclear Clustering of Mitochondria in Cardiac Biopsy-Proven Allograft Rejection. *J. Pers Med.* 12 (2), 296.
- Tonnesmann, E., Kandolf, R., Lewalter, T., 2013. Chloroquine cardiomyopathy—a review of the literature. *Immunopharmacol Immunotoxicol.* 2013 (35), 434–442. <https://doi.org/10.3109/08923973.2013.780078>.
- Tselios, K., Gladman, D.D., Harvey, P., Akhtari, S., Su, J. & Urowitz, MB., 2019. Abnormal cardiac biomarkers in patients with systemic lupus erythematosus and no prior heart disease: a consequence of anti-malarials? *J. Rheumatol.* 46 (1), 64–69. <https://doi.org/10.3899/jrheum.171436>.
- Vilahir, G., Juan-Babot, O., Pena, E., Onate, B., Casani, L. & Badimon, L., 2011. Molecular and cellular mechanisms involved in cardiac remodeling after acute myocardial infarction. *J. Mol. Cell Cardiol.* 2011 (50), 522–533. <https://doi.org/10.1016/j.yjmcc.2010.12.021>.
- Wick, R.M., 2019. The hematoxylin and eosin stain in anatomic pathology—An often-neglected focus of quality assurance in the laboratory. *Seminars in Diagnostic Pathology.* 36 (5), 303–311. <https://doi.org/10.1053/j.semmp.2019.06.003>.
- Xu, Z., Kim, S., Huh, J., 2014. Zinc plays a critical role in the cardio-protective effect of post conditioning by enhancing the activation of the RISK pathway in rat hearts. *Journal of Molecular and Cellular Cardiology* 66 (2014), 12–17. <https://doi.org/10.1016/j.yjmcc.2013.10.016>.
- Ye, J., Zhang, B., Xu, J., Chang, Q., McNutt, M.A., Korteweg, C., Gong, E., et al., 2007. Molecular pathology in the lungs of severe acute respiratory syndrome patients. *Am J Pathol* 170, 538–545.
- Zhou, Y., Pan, P., Yao, L., Su, M., He, P., Niu, N., McNutt, M., Gu, J., 2010. CD117-positive Cells of the Heart: Progenitor Cells or Mast Cells? *J Histochem Cytochem.* 58 (4), 309–316.
- Wagner, M.J., Khan, M., Mohsin, S., 2020. Healing the Broken Heart; The Immunomodulatory Effects of Stem Cell Therapy. *Front. Immunol.* 11, 639. <https://doi.org/10.3389/fimmu.2020.00639>.

Further Reading

- Hayat, M.A., 2000. *Principles and techniques of electron microscopy: biological applications*. Cambridge University Press, Cambridge, pp. 546–548.